ADVANCED HEALTHCARE MATERIALS
www.advhealthmat.de

Design of Recombinant Spider Silk Proteins for Cell Type Specific Binding

*Vanessa Tanja Trossmann and Thomas Scheibel**

Cytophilic (cell-adhesive) materials are very important for tissue engineering and regenerative medicine. However, for engineering hierarchically organized tissue structures comprising different cell types, cell-specific attachment and guidance are decisive. In this context, materials made of recombinant spider silk proteins are promising scaffolds, since they exhibit high biocompatibility, biodegradability, and the underlying proteins can be genetically functionalized. Here, previously established spider silk variants based on the engineered *Araneus diadematus* fibroin 4 (eADF4(C16)) are genetically modified with cell adhesive peptide sequences from extracellular matrix proteins, including IKVAV, YIGSR, QHREDGS, and KGD. Interestingly, eADF4(C16)-KGD as one of 18 tested variants is cell-selective for C2C12 mouse myoblasts, one out of 11 tested cell lines. Co-culturing with B50 rat neuronal cells confirms the cell-specificity of eADF4(C16)-KGD material surfaces for C2C12 mouse myoblast adhesion.

1. Introduction

Cells are enveloped in a complex and dynamic microenvironment including an extracellular matrix (ECM), soluble factors, and neighboring cells decisive for cellular responses and functions.[1] The ECM is an essential regulator of cell behavior, since it provides interaction sites for cells important for physical and mechanical support.[2] Due to the regulatory effects of the ECM,[3] tissue engineering aims to generate artificial, biomimetic matrix substitutes, which maintain, support, or restore the regeneration of tissues.[4] Therefore, either biofunctionalized, acellular scaffolds, or pre-cultured tissue constructs combining cells and artificial ECM materials are used to promote tissue regeneration and formation.[5] Tissue-specific elements should be implemented to construct a biomimetic extracellular microenvironment imitating the natural one.[6] Ideally, an artificial scaffold supports a guided and selective interaction of tissue-specific cells to enable the formation of hierarchically organized tissue structures.[5e,f,j,7] Functionalization using stimulating growth factors, ECM proteins or active fragments and peptides thereof is widely used to design bioactive surfaces to control cellular responses.[5e,f,j,7d,8]

The cell adhesive activity of the tripeptide Arg–Gly–Asp (in one letter code: RGD) has been identified in the 1980s, and this sequence can be found in different ECM proteins, such as fibronectin, representing a prime example for a minimal necessary peptide sequence recognized by cellular receptors (integrins).[9] This decisive discovery has enabled the development of functionalized materials to promote cell interactions.[5j,8h,10] Since RGD is a peptide sequence recognized by various integrin receptors, it interacts with many cell types.[11] However, selective attachment and growth of desired cells and simultaneous non-adhesion of other cells are crucial factors to generate hierarchically structured tissue constructs. Besides RGD, other cell-binding peptides sequences have been identified over time stimulating cellular responses and enabling the generation of cell-contacting surfaces.[5f,j,7a,d,8g,h,12] Some examples of other cell adhesive peptides are Ile–Lys–Val–Ala–Val (IKVAV) derived from laminin,[13] Tyr–Ile–Gly–Ser–Arg (YIGSR) derived from laminin,[14] Lys–Gly–Asp (KGD) derived from collagen and barbourin,[15] Gly–Phe–Hyp–Gly–Glu–Arg (GFOGER) derived from collagen,[16] Gln–His–Arg–Glu–Asp–Gly–Ser (QHREDGS) derived from angiopoietin,[17] Arg–Glu–Asp–Val (REDV) derived from fibronectin,[18] or Asp–Gly–Glu–Ala (DGEA) again derived from collagen.[19]

Materials made of the engineered recombinant spider silk protein Araneus diadematus fibroin 4 (eADF4) and its variants have been shown to be promising candidates for tissue engineering due to their low inflammatory properties, good biocompatibility, and possible biodegradability.[20] Specific genetic engineering

V. T. Trossmann, T. Scheibel
Chair of Biomaterials
Engineering Faculty
University of Bayreuth
Prof.-Rüdiger-Bormann-Straße 1, 95447 Bayreuth, Germany
E-mail: thomas.scheibel@bm.uni-bayreuth.de
T. Scheibel
Bayreuth Center for Colloids and Interfaces (BZKG)
Bavarian Polymer Institute (BPI)
Bayreuth Center for Molecular Biosciences (BZMB)
Bayreuth Center for Material Science (BayMAT)
University of Bayreuth
Universitätsstraße 30, 95447 Bayreuth, Germany

The ORCID identification number(s) for the author(s) of this article can be found under https://doi.org/10.1002/adhm.202202660

DOI: 10.1002/adhm.202202660

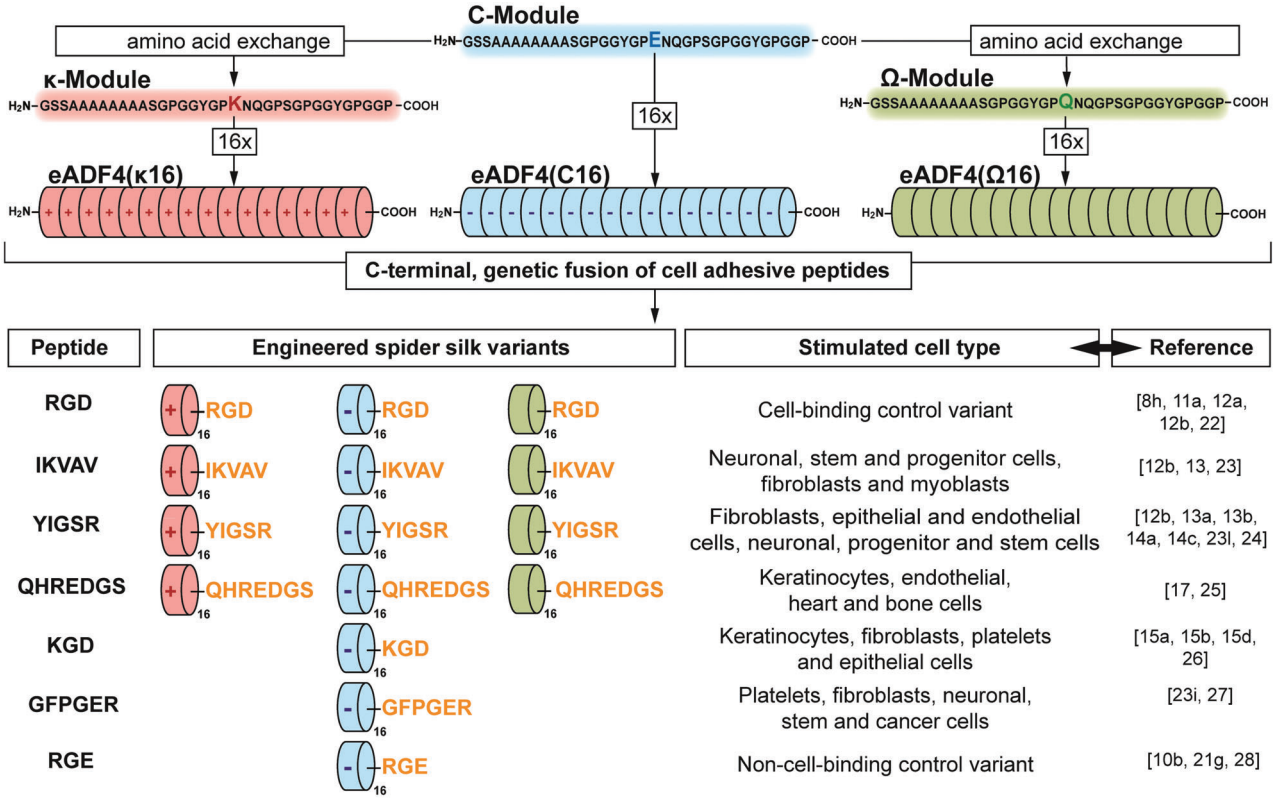

Figure 1. Design of recombinant spider silk proteins based on Araneus diadematus fibroin 4 (ADF4) carrying cell binding peptides for cell type specific interaction. The consensus sequence of ADF4 inspired the engineering of the C-module for recombinant production. In κ- or Ω-modules, the negatively charged glutamic acid (E) residues have been replaced by either positively charged lysine (K) or uncharged glutamine (Q) residue, respectively. The appropriate recombinant engineered spider silk proteins eADF4(C16) (negative net charge), eADF4(κ16) (positive net charge), and eADF4(Ω16) (neutral net charge) comprise 16 repeats of the respective modules. Cell binding peptides identified in the depicted references were genetically fused to the C-terminal end of the respective protein. IKVAV, YIGSR, QHREDGS, KGD, and GFPGER were selected due to their reported cell-specific stimulating effects (Table 1). RGD- and RGE-tagged variants served as well-established cell-binding and non-cell-binding controls, respectively.

of the recombinant protein enables a task-specific functionalization of materials made thereof.[21] In the present study, new recombinant spider silk proteins were modified with peptide tags for guided cell attachment. The cell adhesive peptides IKVAV, YIGSR, QHREDGS, KGD, and GFPGER were each genetically fused to previously established eADF4(C16), eADF4(κ16), and eADF4(Ω16) (**Figure 1**). After recombinant production and characterization, the obtained 18 spider silk proteins were processed into films, analyzed concerning cell adhesion using 11 different mammalian cell types and categorized into cell-adhesive (cytophilic), non-cell-adhesive (cytophobic), and cell-selective variants.

2. Results and Discussion

2.1. Production and Characterization of New Spider Silk Variants

The consensus sequence of the repetitive core motif of *Araneus diadematus* fibroin 4 (ADF4) has been used as template for the engineered recombinant spider silk variants eADF4(C16) (negatively charged),[21a] eADF4(κ16) (positively charged),[21b] and eADF4(Ω16) (uncharged).[21c,d] These variants have been previously modified with RGD-tags to enhance cell attachment.[21e,g] Here, the eADF4-based spider silk proteins were functionalized with further cell-interaction peptides due to a previously reported cell-type specificity allowing guided and selective cell attachment (**Table 1** and Figure 1).

In case of the collagen-derived GFOGER tag, a proline (P) residue was part of the sequence instead of the naturally occurring hydroxy-proline (O) due to the recombinant production of this spider silk variant using *Escherichia coli* (*E. coli*) bacteria, which lack the enzymes for respective post-translational modifications.[29] Recombinant production was successful for all 18 spider silk variants used in our experiments (Figure 1).[21a–e,g] Table S1, Supporting Information, summarizes important protein parameters including the number of charged amino acid residues, the isoelectric point, or the molecular weight (MW). For uncharged eADF4(Ω16) variants, the influence of charged amino acid tags on the isoelectric point is more pronounced than for negatively charged eADF4(C16) or positively charged eADF4(κ16) spider silk proteins. Since the addition of peptides increases the MW by around 1000 Da (i.e., only around 2 % of the MW), the physico-chemical properties, except the desired cell interaction and stimulation, should be driven by the underlying spider silk protein. The correct gene expression and high purity of produced eADF4-based variants could be confirmed using

Table 1. Reported biological effects of peptides used herein. Besides the cytophilic RGD sequence, other cell-interaction peptides showing cell-type specificity were used in this study to allow guided and selective cell attachment.

Peptide	Origin	Biological Effect	References
RGD	Fibronectin	Activation of different integrin receptors enabling increased adhesion, spreading, proliferation, migration, and differentiation of various cell types including stem cells	[8h, 11a, 12a,b, 22]
IKVAV	Laminin	Increased attachment, proliferation, viability, and differentiation of neuronal cells, neuronal progenitor cells as well as stem cells; enhanced neurite growth and extension; attachment of fibroblasts; adhesion, growth and differentiation of myoblasts; adhesion and growth of cancer cells	[12b, 13, 23]
YIGSR	Laminin	Improved adhesion, spreading, migration, and growth of endothelial cells; attachment, spreading, and stress fiber formation of fibroblasts; increased adhesion and extension of epithelial cells; enhanced adhesion, growth, viability, and differentiation of neuronal cells, neuronal progenitor cells and stem cells; enhanced neurite growth and extension; interaction of cancer cells	[12b, 13a,b, 14a,c, 23l, 24]
QHREDGS	Angiopoietin	Enhanced endothelial cell survival, metabolism, and tube formation; promoted survival of heart cells; polarization of macrophages; attachment and survival of keratinocytes; inhibited apoptosis of stem cells; enhanced osteoblast differentiation, bone matrix deposition, and mineralization	[17, 25]
KGD	Collagen	Enhanced keratinocyte adhesion and spreading; reduced platelet aggregation; enhanced epithelial cell and fibroblast adhesion	[15a,b,d, 26]
GFOGER	Collagen	Increased adhesion of platelets and human neuronal stem/progenitor and fibrosarcoma cells; chondrogenic differentiation of human bone mesenchymal stem cells; adhesion and spreading of fibroblasts	[23i, 27]
RGE	Control	No cell attachment including fibroblasts and endothelial cells	[10b, 21g, 28]

matrix-assisted laser desorption/ionization mass spectrometry with time-of-flight (MALDI-TOF) analysis (Table S1 and Figure S1, Supporting Information) as well as silver-stained sodium dodecyl sulfate polyacrylamide gel electrophoresis (SDS-PAGE), fluorescence, and circular dichroism (CD) spectroscopy (Figure S2, Supporting Information). MALDI-TOF spectra showed one sharp peak around the expected MW for all variants (Figure S1, Supporting Information). Minor variations could result from natural measurement fluctuations and possible ionic interactions (e.g., Na^+) with the matrix.[30] Silver-stained SDS-PAGs (Figure S2A, Supporting Information) displayed single bands at a MW of around 65 kDa for eADF4(C16)-, at around 48 kDa for eADF4(κ16)- and at around 55 kDa for eADF4(Ω16)-based variants. Incomplete and irregular binding capacities of negatively charged SDS to differently charged recombinant spider silk proteins led to a different charge distribution and explained the different migration behavior of these variants.[21a] Since tyrosine-rich recombinant spider silk proteins contain no tryptophan, but *E. coli* proteins comprise on average 1.5 % Trp residues,[21a,31] protein purity could be confirmed using fluorescence spectroscopy indicating the absence of an intrinsic Trp (347 nm) and the presence of a high Tyr (303 nm) fluorescence signal (Figure S2B, Supporting Information). Furthermore, regardless of fused peptides, far-UV CD spectra verified the random coil secondary structure in solution for all 18 variants, indicated by a broad minimum around 205 nm and a plateau around 219 nm (Figure S2C, Supporting Information).[21a,g,32]

2.2. Analysis of Spider Silk Films regarding Cell Type Specific Adhesion

Spider silk films (0.5 mg protein per 1 cm^2) were produced using drop-casting on polystyrene surfaces followed by post-treatment using ethanol vapor to induce β-sheet formation making the films water insoluble, but preserving surface exposition of the peptide tags as reported previously.[21e,g,32,33] Since surface hydrophobicity influences protein and cell interaction, water contact angles (WCA) were determined and revealed that all 18 spider silk films provided hydrophilic surfaces (WCA below 90°) (Figure S3, Supporting Information).[21f,34]

Table 2. Cell type, tissue origin, and reasons for the selection of the cells. Abbreviations: HUVECs: human umbilical vein endothelial cells, hiPSC-CMs: human induced pluripotent stem cell derived cardiomyocytes.

Cell type	Tissue Origin	Reason
BJ fibroblasts	Human skin	GFPGER, KGD, YIGSR, IKVAV
Balb 3T3 fibroblasts	Mouse embryo	GFPGER, KGD, YIGSR, IKVAV
C2C12 myoblasts	Mouse muscle	IKVAV
HaCaT keratinocytes	Human skin	KGD, QHREDGS
B50 neuronal cells	Mouse nerve	IKVAV, YIGSR
RN22 Schwann cells	Rat nerve	IKVAV, YIGSR
NG108 cell hybrids	Rat-mouse nerve	IKVAV, YIGSR
HeLa epithelial cells	Human cervix carcinoma	IKVAV, YIGSR
HUVECs	Human vascular system	QHREDGS, YIGSR
hiPSC-CMs	Human heart	QHREDGS, IKVAV
MG63 fibroblasts	Human osteosarcoma	QHREDGS, GFPGER

To analyze specific cell interactions as described in literature (Table 1), all spider silk films were investigated regarding the adhesion behavior (t = 4 h) of 11 different mammalian cell lines originating from several tissues (**Table 2**). Cell attachment was analyzed in absence and presence of fetal calf serum (FCS) or comparable supplements to screen influences of adsorbed serum proteins on cell adhesion.[23l,28,35]

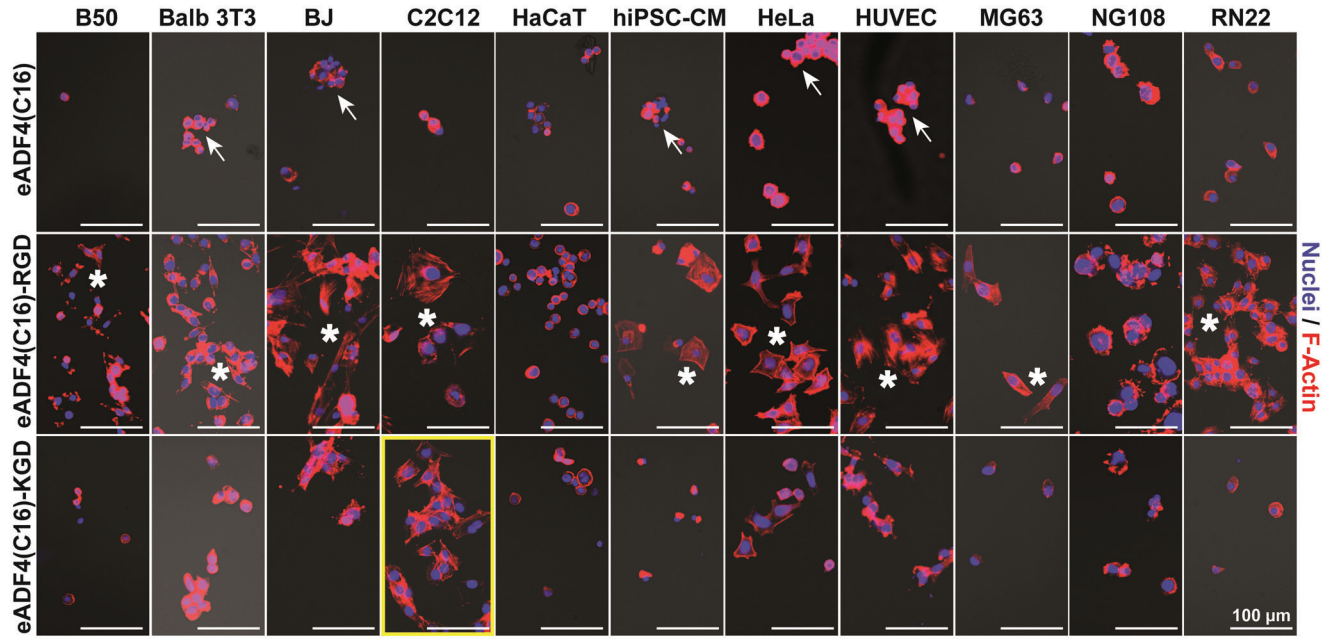

Figure 2. Cell adhesion on films made of eADF4(C16) (cytophobic), eADF4(C16)-RGD (cytophilic), and eADF4(C16)-KGD (cell selective). Cell adhesion and spreading of rat B50 neuronal cells, mouse Balb 3T3 embryonal fibroblasts, human BJ fibroblasts, mouse C2C12 myoblasts, human HaCaT keratinocytes, human induced pluripotent stem cell derived cardiomyocytes (hiPSC-CM), human HeLa cervix carcinoma cells, human umbilical vein endothelial cells (HUVEC), human MG63 bone fibroblasts, mouse-rat NG108 neuronal hybrid cells, and rat RN22 Schwann cells on different spider silk films were recorded after 4 h of incubation using fluorescence microscopy. Therefore, cell nuclei and F-actin cytoskeleton of fixed cells were stained using DAPI (blue) and Phalloidin (red), respectively. White arrows point towards round cellular aggregates showing small cell body sizes and preferring cell–cell-contacts, but no/little cell–matrix interactions. White asterisks highlight clearly spread cells exhibiting enhanced cell body sizes. The yellow box marks the selectivity of C2C12 myoblasts on the eADF4(C16)-KGD variant. Scale bars: 100 µm.

After 4 h of incubation, cell nuclei (4′,6-diamidino-2-phenylindole, DAPI, blue) and the F-actin cytoskeleton (phalloidin–rhodamine B, phalloidin, red) of adhered cells were visualized using fluorescence staining to determine, if a spider silk variant shows a cytophobic or a cytophilic character. Cytophobicity does not equate with cytotoxicity, since recombinant eADF4-based spider silk materials are highly biocompatible, non-cytotoxic, and cause no inflammatory or allergic reaction.[20b,36] The cytophilicity of spider silk variants was classified as very good (++), good (+), moderate (0), bad (−), and very bad (−) regarding the total number of attached cells, their spreading behavior and the cell body size. Cytophobic spider silk surfaces were characterized by a low number of sporadically distributed cells exhibiting a round morphology with a low F-actin expression resulting in a small cell body size. Moreover, cells could not form proper, adequate cell-material adhesions leading to a reduced surface attachment and formation of cellular aggregates or clusters comprising several individual cells, which prefer cell-to-cell contacts compared to cell–matrix-interactions. In contrast, on cytophilic surfaces, many cells adhered uniformly distributed and showed a clear F-actin expression with identifiable filaments of the cytoskeleton and distinct focal adhesions leading to clearly enhanced cell spreading. On moderately cytophilic surfaces some small cell aggregates as well as some partially spread cells were visible exhibiting a round morphology with reduced cell body size and some F-actin expression indicated as stress fibers.

Figure 2 shows representative fluorescence images of all cell types on spider silk surfaces made of the cytophobic eADF4(C16), the cytophilic eADF4(C16)-RGD, and eADF4(C16)-KGD in presence of FCS. Furthermore, cell numbers of four selected, representative fluorescence images per eADF4(C16), eADF4(C16)-RGD, and eADF4(C16)-KGD were counted for every cell line and summed up to quantify cell adhesion behavior on these spider silk variants (Figure S5, Supporting Information). It was expected that eADF4(C16) films would be cytophobic, since the amino acid sequence of eADF4(C16) lacks any cell binding motifs.[21e,g,33,36b,37] This assumption could be verified, because the few detected cells displayed a round, less spread morphology showing F-actin expression mainly around the cell nuclei. Either sporadically distributed cells, for example, for B50 neuronal or MG63 osteosarcoma cells, or cellular aggregates, as seen for Balb 3T3 and BJ fibroblasts, human induced pluripotent stem cell (hiPSC)-CM, HeLa cells, or human umbilical vein endothelial cells (HUVEC), were visible (Figure 2, white arrows). RN22 Schwann cells seemed to be an exception, since more cells attached (Figure S5, Supporting Information). These cells formed F-actin containing stress fibers for mechanotransduction and migration instead of focal adhesions. Importantly, due to the low cell amount, non-specific cell attachment based on serum protein adsorption could be excluded.

Since RGD is a widespread and abundant cell (integrin) interaction peptide used for enhancing cytophilicity of biomaterials,[8g,h,10b,11c,38] strong cell interaction with

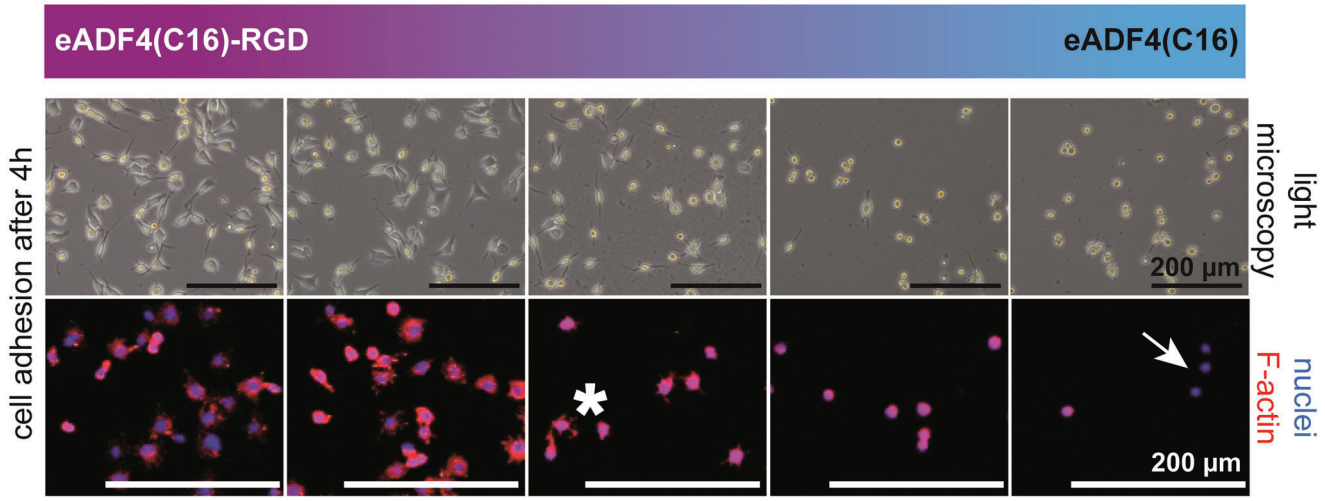

Figure 3. Adhesion of Balb 3T3 fibroblasts on a gradient film from eADF4(C16)-RGD towards eADF4(C16) after 4 h of incubation. Cell adhesion with increasing availability of cell interaction peptide was analyzed after 4 h using light microscopy (before washing) and confocal microscopy after washing, fixing, and staining the attached cells. Cell nuclei and F-actin cytoskeleton were stained using DAPI (blue) and Phalloidin (red), respectively. The white arrow points towards round, only DAPI-stained cells without any F-actin expression. The white asterisk highlights cells starting to form focal adhesions and F-actin stress fibers. Scale bars: 200 µm.

eADF4(C16)-RGD surfaces was expected.[21e,g,39] For all investigated cell types, high cell numbers and a spread morphology with F-actin-containing focal adhesions could be detected on eADF4(C16)-RGD (Figure 2, white asterisks). HaCaT keratinocytes always exhibited a round morphology with a uniform F-actin expression around the cell nuclei, since they need proper cell–cell-contacts. Due to the short incubation time, NG108 hybrid cells did not outgrow any neurites or axons. Other studies using RGD-modified spider silk surfaces confirmed high cytophilicity of this peptide.[23l,35e,40]

The silk-specific adhesion of murine Balb 3T3 fibroblasts was further evaluated on gradient films made of eADF4(C16) and eADF4(C16)-RGD after 2 h (Figure S4A, Supporting Information) and 4 h (**Figure 3**) in comparison to eADF4(C16), eADF4(C16)-RGD, and glass controls (Figure S4B, Supporting Information). Confocal images revealed only little cell numbers, some did not even show any F-actin expression (Figure 3 and Figure S4, white arrows, Supporting Information), attached at areas consisting of mainly eADF4(C16), and most of these round cells could be washed off. With increasing eADF4(C16)-RGD content, presumably at a 50:50 ratio, the first focal adhesions and F-actin stress fibers appeared and cell spreading enhanced (Figure 3 and Figure S4, white asterisks, Supporting Information). It was concluded that around 75% w/w of eADF4(C16)-RGD content is sufficient to enable complete cell attachment. Other studies using RGD gradients also showed improved cell attachment and spreading with increasing RGD ligand density.[41]

The collagen-derived KGD peptide tag was chosen to enhance interactions with keratinocytes, fibroblasts, and epithelial cells.[15a,b,d,26] Interestingly, here, eADF4(C16)-KGD films were highly selective for C2C12 myoblasts, which attached in a spread morphology with F-actin containing focal adhesions comparable to eADF4(C16)-RGD (Figure 2, yellow box), while other cell types showed less interactions (Figure S5, Supporting Information). In presence of FCS, the eADF4(C16)-KGD variant provided a moderate primary interaction surface for some cells (e.g., Balb 3T3, BJ, HeLa, and HUVEC), whereas the other investigated cell lines (B50, HaCaT, hiPSC-CM, MG63, NG108 and RN22) showed similar responses as seen on eADF4(C16) surfaces.

All film- and cell-interactions were visualized using bar charts (**Figure 4**). Based on our results, eADF4(C16), eADF4(C16)-RGE, eADF4(C16)-GFPGER, and eADF4(Ω16) were categorized as cytophobic spider silk variants. These results verified the expectations, since eADF4(C16)-RGE was used as a non-cell-binding control variant[21g,42] and the uncharged eADF4(Ω16), like negatively charged eADF4(C16), does not contain cell interaction sites.[21e,37a,43] The exchange of post-translationally modified hydroxy-proline (GFOGER) to proline (GFPGER) residues obviously also reduced cell binding properties.

Polycationic material surfaces are known to enhance unspecific cell-material interactions due to serum protein adsorption as well as higher affinity of mostly negatively charged cell membrane components.[33,44] Here, our positively charged spider silk variants also enhanced cell interactions and cytophilicity. Previous studies have already shown that positively charged eADF4(κ16) displayed enhanced cell-stimulation behavior compared to negatively charged eADF4(C16) and uncharged eADF4(Ω16) materials.[21e,h,33,37b] Many cell types already showed improved adhesion and spreading on eADF4(κ16) surfaces in presence as well as absence of FCS. Thus, although some FCS-related, cell-type specific effects (e.g., Balb 3T3 or hiPSC-CM adhesion on eADF4(κ16) or Balb 3T3 and RN22 attachment on eADF4(C16)) were visible, unspecific cell adhesion to surface-adsorbed serum proteins played a subordinate role on these spider silk surfaces.

The laminin-derived IKVAV peptide was expected to interact mainly with neuronal cells, but also fibroblasts, myoblasts, or cancer cells.[12b,13,23] eADF4(κ16)-IKVAV films were cytophilic for many cell types. Although eADF4(κ16)-IKVAV showed no FCS effect, the absence or presence of serum proteins or sup-

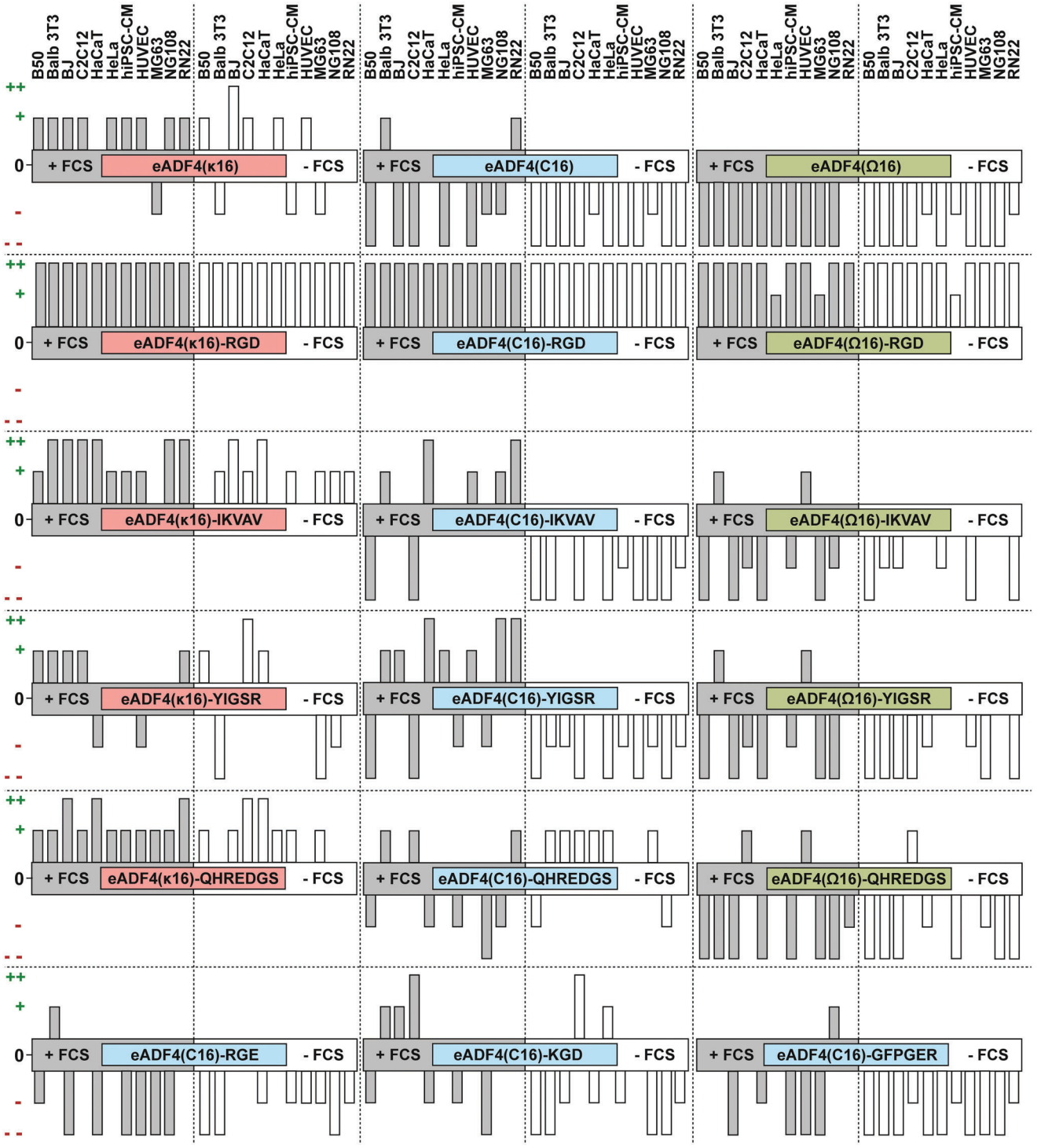

Figure 4. Adhesion of mammalian cell lines on films made of different recombinant spider silk proteins after 4 h of incubation. 11 cell lines were incubated on 18 different spider silk films in the absence or presence of FCS. Adhesion after 4 h of incubation was analyzed using fluorescence microscopy after fixing and staining attached cells. The adhesion was ranked as follows by the number of attached cells and their spreading behavior: very good (++), good (+), neutral (0), bad (−), and very bad (−).

plements could be used to selectively guide cellular attachment on eADF4(C16)-IKVAV and eADF4(Ω16)-IKVAV surfaces. There, the IKVAV peptide seemed to promote primary attachment of Balb 3T3 fibroblasts, HUVECs as well as selected neuronal cells (e.g., NG108 hybrid and RN22 Schwann cells).

The laminin-derived YIGSR peptide has been shown to stimulate neuronal cells, endothelial cells, fibroblasts, keratinocytes, and cancer cells.[12b,13a,b,14a,c,23l,24] Interestingly, the charge effect of eADF4(κ16)-YIGSR was not as strong as on the other positively charged eADF4(κ16) variants, but a clear FCS effect could be identified in case of this variant. While Balb 3T3 fibroblasts and C2C12 myoblasts adhered to eADF4(κ16)-YIGSR in presence of FCS, only C2C12 myoblasts remained their strong cell attachment in absence of serum. FCS addition also enabled a cell-type specific adhesion on eADF4(C16)-YIGSR and eADF4(Ω16)-YIGSR surfaces. Since HaCaT keratinocytes, RN22 Schwann, NG108 hybrid cells, HUVECs, Balb 3T3, and BJ fibroblasts showed good attachment on eADF4(C16)-YIGSR films, this variant could also be used for neuronal or skin tissue engineering.

The angiopoietin-derived QHREDGS peptide tag should enhance interaction of surfaces with endothelial cells, cardiomyocytes, myoblasts, stem cells, or bone cells.[17,25] The cytophilicity of positively charged eADF4(κ16)-QHREDGS mainly resulted from the already known charge effect. However, the QHREDGS modification seemed to stimulate C2C12 myoblast attachment charge-independently. Furthermore, eADF4(C16)-QHREDGS showed FCS-influenced cell type selectivity, since attachment of MG63 bone fibroblasts and HaCaT keratinocytes was reduced in presence and enhanced in absence of supplements. HUVECs exhibited a moderate or good attachment behavior on the QHREDGS-modified spider silk variants indicating to some extent an interaction of cell surface receptors with the surface.

The shown systematic evaluation classified eADF4(C16)-RGD as cytophilic, eADF4(C16)-KGD as cell-selective, and eADF4(C16)-RGE as cytophobic, clearly demonstrating how sensitive cellular receptors recognize peptide sequences and interact with specific amino acid sequences, although only one amino acid residue differs. The modification of eADF4(C16) with RGD, RGE, and KGD sequences allowed the analysis regardless of charge effects, since the proteins exhibited identical physico-chemical properties due to similar charge distribution (one positively charged arginine [R] or lysine [K] and one negatively charged glutamic acid [E] or aspartic acid [D]). For RGE, the exchange of aspartic acid (D) with glutamic acid (E) increased the length of the side group by one CH_2-unit leading to a reduced cell interaction[21g,23l,28b,42b,45] explained by a reduced binding affinity due to steric hindrance inside the integrin binding pocket.[10b] Several integrin receptors recognize and bind RGD[11a,12a,46] and some are also able to bind KGD.[47] The binding affinity of RGD-specific integrins could be lower for KGD due to the shorter lysine (K) versus arginine (R) residue leading to a cell-type dependent interaction explaining the divergent cell attachment behavior.[47] However, it is also assumed that C2C12 myoblasts express cellular receptors, which are able to specifically interact with KGD. The $\alpha_5\beta_1$ and the $\alpha_v\beta_1$ integrins, both binding RGD,[46a] also interact with the ectodomain of collagen XVII, which contains several KGD peptide sequences.[15b,46b,47] Furthermore, several studies have shown that snake venom poisons containing KGD peptide sequences could interact with cellular surface receptors, for instance $\alpha_{IIb}\beta_3$ and $\alpha_5\beta_1$.[15a,c,26a,48] However, receptor affinity and specificity as well as successful integrin–peptide interactions are strongly influenced by the amino acid following the important recognition sequence. While a KGDW sequence promoted $\alpha_{IIb}\beta_3$-binding, a KGDD sequence showed enhanced interaction with the $\alpha_5\beta_1$ integrin.[15a,c] Furthermore, KGDK and KGDR showed strong interaction with $\alpha_5\beta_1$ and the $\alpha_v\beta_1$ integrins, while KGDM and KGDQ were less efficient.[15b] In our case, the serine-residue that follows the KGD sequence seems to beneficially support the interaction with surface receptors of C2C12 myoblasts.

The subsequent amino acid residues are also decisive for integrin affinity and specific cell attachment to RGD[5j,8h,11b,35e,49] and YIGSR- or IKVAV-containing peptides.[13a,c,14c] Since these studies confirmed the importance of specific amino acid residues upfront and after the appropriate cell recognition site, the cell interaction and specificity of the here presented spider silk variants could also be an effect of the flanking amino acid residues.

2.3. Selective Myoblast Attachment on eADF4(C16)-KGD Films in Co-Culture

Since in natural tissue (e.g., muscle tissue) a heterotypic communication between cells occur, different co-culture systems combining, for instance, myoblasts with endothelial cells[50] or fibroblasts[51] have been evolved to improve cellular responses. Moreover, previously published studies have shown that the co-culture of neural cells and muscle cells has stimulating effect on both cell types and promotes the formation of functional muscle or neuronal tissue.[52] However, since adhesion and growth of tissue-specific cells are decisive for generating hierarchically organized tissue structures, the selective cell attachment of C2C12 myoblasts on eADF4(C16)-KGD was demonstrated in a co-culture model with B50 neuronal cells and eADF4(C16)-RGD as a control (**Figure 5**). The described cell-specific serum/supplement effect was used to enhance selective C2C12 attachment, while simultaneously prohibiting B50 adhesion. After washing off unattached cells, the adhered cells were incubated in full media. The specific, time-dependent life cell tracking yielded green fluorescing C2C12 myoblasts (Syto 9) and red fluorescing B50 neuronal cells (Red CMTPX) in single and co-culture experiments on spider silk films directly after seeding (Figure 5). However, some B50 neuronal cells displayed no fluorescence indicating no uptake of the dye (Figure 5, white triangles). Both fluorescence dyes are membrane permeable, but not permanently integrated inside the cells. The red CMTPX dye is supposed to be metabolized into non-cell membrane permeable products inside the cell, and the DNA intercalating Syto 9 dye should only show high fluorescence signals after contact with nucleic acids. Thus, only cells with ingested dyes showed fluorescence as confirmed by the low background signal. Yellow cross-signals can occur if differently stained cells are arranged on top of each other and their fluorescence signals overlap.[52g] However, despite several washing steps, some dye molecules might also have interacted with the cell surface and could be released into the cell culture media triggered by osmosis and diffusion. Thus, the subsequent uptake

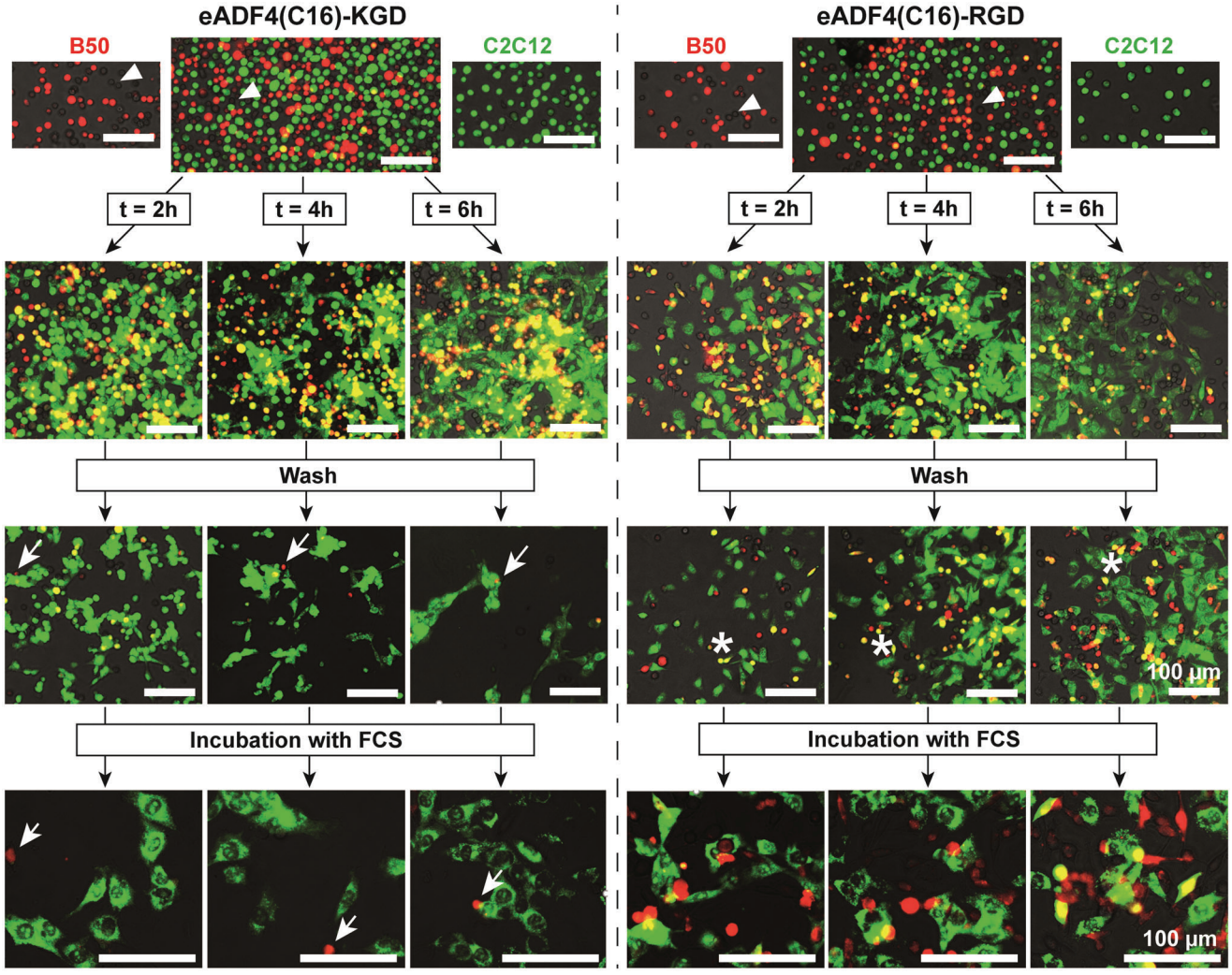

Figure 5. Selective attachment and spreading of C2C12 mouse myoblasts and detachment of B50 rat neuronal cells upon incubation on films made of eADF4(C16)-KGD. Labeled C2C12 mouse myoblasts (green) and B50 rat neuronal cells (red) were incubated for 2, 4, or 6 h on films made of eADF4(C16)-KGD and eADF4(C16)-RGD in the absence of FCS. After washing with 1× PBS, only C2C12 myoblasts were attached on eADF4(C16)-KGD films, while B50 neuronal cells could not attach to this silk variant and were washed off. In contrast, on eADF4(C16)-RGD films both cell lines could attach and spread. After further 20–24 h of incubation in presence of FCS, cells were still attached. On eADF4(C16)-KGD surfaces a selective growth of C2C12 myoblasts was possible. White triangles highlight unlabeled B50 cells. White arrows point towards sporadically attached, remaining red stained B50 neuronal cells on eADF4(C16)-KGD. White asterisks highlight cells showing a yellow fluorescence cross signal after uptake of both dyes. Scale bars: 100 µm.

of an opposite dye by a cell is possible, also resulting in a yellow fluorescence cross-signal (Figure 5, white asterisks).

After 2, 4, and 6 h incubation time, individual wells containing the co-culture were washed with phosphate buffered saline (PBS) to remove unattached cells, and incubated in fresh FCS-containing media (Dulbecco's modified Eagle's medium [DMEM]) overnight to ensure survival of the remaining cells. Subsequent fluorescence microscopy revealed that on eADF4(C16)-KGD films primarily myoblasts (Figure 5, green cells) adhered and spread, while only a few round, non-spread B50 neuronal cells (Figure 5, red cells, white arrows) could be identified. In contrast, both cell types adhered and spread on cytophilic eADF4(C16)-RGD, which consequently led to a higher yellow fluorescence cross-signal. The apparently larger area of green fluorescence could be explained by the larger cell body size of spread C2C12 myoblasts compared to B50 neuronal cells, which was also noticeable in single culture after nuclei and F-actin staining (Figure 3).

After initial cell attachment, cell proliferation is an important pre-requisite for successful tissue engineering requiring nutrients, growth factors, and soluble plasma proteins present in FCS or comparable supplements. Thus, cell proliferation of seven cell lines from different mammalian tissues was investigated conducting a cell titer blue assay over 8 days on eADF4(C16), eADF4(C16)-RGD, and eADF4(C16)-KGD films to confirm selective proliferation of C2C12 myoblasts on KGD-functionalized surfaces (Figure S6, Supporting Information). The cytophobic character of eADF4(C16) could be verified, because none of the investigated cell lines grew. In contrast, the high cytophilicity of eADF4(C16)-RGD was confirmed, since the cell number of all

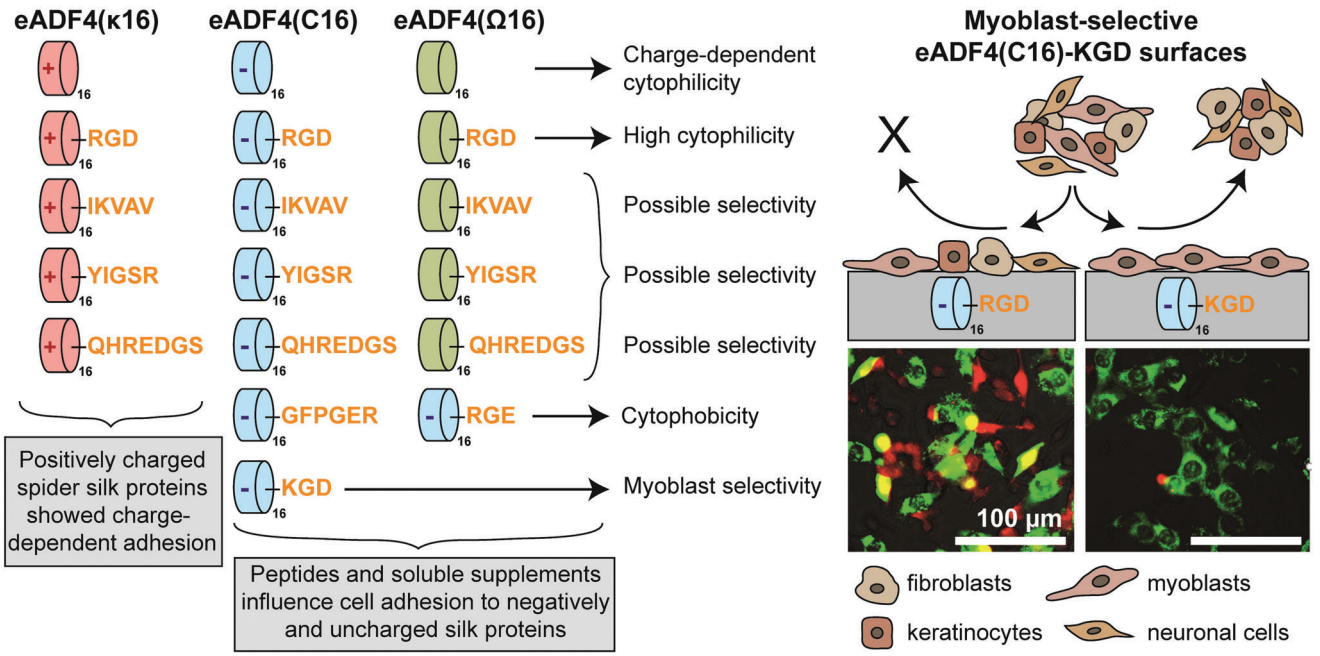

Figure 6. Summary of identified cellular responses to different spider silk variants. Non-tagged eADF4-based spider silk variants showed a charge-dependent cytophilicity, which could be enhanced by introducing the RGD-sequence. Generally, positively charged eADF4(κ16)-surfaces improved cell adhesion, while specific peptide tags mainly influenced cell adhesion on negatively and uncharged eADF4(C16)- and eADF4(Ω16)-variants. Although IKVAV-, YIGSR-, and QHREDGS-surfaces showed possible cell type selectivity, eADF4(C16)-KGD was identified as a myoblast-specific spider silk variant allowing selective cell attachment.

cell lines increased over the investigated incubation time. Since only C2C12 myoblasts displayed proliferation on eADF4(C16)-KGD films and the other cell lines behaved as on eADF4(C16), cell selective behavior of this variant was verified. These results also confirmed that cell attachment and cell proliferation are different cellular responses, since BJ fibroblasts showed good cell attachment (Figures 2 and 4), but no proliferation on the eADF4(C16)-KGD surface.

3. Conclusion

The present study showed that genetic modification of recombinant spider silk proteins enables the processing of cell type specific silk materials (**Figure 6**). In general, a charge-dependent cytophilicity of non-tagged eADF4-based spider silk variants was visible, since only positively charged eADF4(κ16) allowed cell adhesion, while negatively charged eADF4(C16)- and uncharged eADF4(Ω16)-films showed a cytophobic character. However, the cytophilicity of these spider silk variants could be increased by introducing the integrin-binding RGD-sequence regardless of protein charge.

Functionalization of recombinant spider silk proteins with other short peptide tags from ECM proteins allowed specific cell attachment. In this context, the peptide tags mainly influenced specific cell interactions with surfaces made of negatively charged eADF4(C16)- and uncharged eADF4(Ω16)-variants, as positively charged eADF4(κ16)-surfaces generally improved cell adhesion. The present study revealed that modifying spider silk proteins with IKVAV-, YIGSR-, and QHREDGS-peptides partly led to cell specific interactions with possible selectivity. However, functionalization with the KGD-peptide allowed selective attachment and growth of myoblasts, which could also be confirmed using a co-culture experiment with neuronal cells (Figure 6). These findings enable a tissue-specific application of engineered spider silk materials. Since spider silk proteins are very versatile and could be processed into different morphologies, the range of possible applications is quite broad. Spider silk films can be used as implant coatings to enhance the performance and integration of supportive implants by improved, selected cellular attachment and ingrowth with simultaneously reduced microbial infection and fibrosis.[21c,d,36b,37c] Furthermore, 3D-printable hydrogel networks with adjustable mechanical properties enable the encapsulation of specific cells in appropriate hydrogels with subsequent processing in adopted 3D structures.[39b,42b,53] Further morphologies with different topographical features are fibers, fiber bundles, or nonwoven meshes, as well as porous foams for the cultivation of cells.[20a,b]

4. Experimental Section

If not stated otherwise, all chemicals were purchased from Carl Roth.

Molecular Cloning: The repetitive core domain of natural ADF4 dragline silk served as model for designing the negatively charged eADF4(C16). For recombinant production using *E. coli*, the consensus sequence, also called C-module (sequence: GSSAAAAAAAAS GPGGYG-PENQGPSGPGGYGPGGP) was repeated 16 times and N-terminally functionalized with a T7 tag for specific detection.[21a] Using this strategy, the positively charged eADF4(κ16),[21b] the uncharged eADF4(Ω16),[21c,d] as well as the C-terminally modified eADF4(C16)-RGD,[21g] eADF4(C16)-RGE,[21g] eADF4(κ16)-RGD,[21e] and eADF4(Ω16)-RGD[21e] variants had been generated previously. For functionalizing recombinant spider

silk proteins with further peptide sequences, codon optimized DNA oligonucleotides (Table S1, Supporting Information) were designed for seamless cloning. Single-stranded oligo-nucleotides (Eurofins Genomics, Germany) were annealed using a temperature gradient (95 to 4 °C, 1 °C min^{-1}) in a thermocycler (Bio-Rad Laboratories, Germany). The digestion with *Bam HI* and *Hind III* restriction enzymes (New England Biolabs GmbH, Germany) enabled insertion into a cloning vector and subsequent ligation with respective spider silk proteins.[21a,g] Successful generation of the appropriate DNA gene constructs was confirmed by sequencing (Eurofins Genomics, Germany).

Recombinant Protein Production: eADF4(C16) was purchased from AMSilk GmbH, Germany. For all other variants, time-dependent fed-batch fermentations using *E. coli BL21 gold (DE3)* were conducted.[21a] While eADF4(C16)-variants[21a] were synthesized for 4 h, eADF4(κ16)-[21b] and eADF4(Ω16)-[21c,d] genes were expressed for 2 h at 30 °C to avoid protein degradation and inclusion body formation. For protein purification,[21a–e,g] cells were disrupted, and residual *E. coli* proteins were separated from heat-stable spider silk proteins using a heat step. After precipitation, washing, and freeze-drying, spider silk proteins were stored at −20 °C.

Protein Analysis: To confirm protein purity, MALDI-TOF analysis, SDS-PAGE with subsequent silver staining, as well as fluorescence and Far-UV CD spectroscopy were conducted.[21a,g] Proteins were dissolved in 6 M guanidinium thiocyanate at room temperature (RT). For MALDI-TOF analysis, the protein solutions were treated with ZipTip C4 pipette tips (Millipore, Germany) to desalt and concentrate the proteins. For elution, a SA-matrix containing 60% acetonitrile and 0.1 % trifluoroacetic acid was used. MALDI-TOF spectra were recorded using a Bruker Daltonics Autoflex (Bruker, Germany) equipped with a 337 nm laser in linear mode and an acceleration voltage between 20 and 40 kV (n = 1). To analyze soluble proteins, silk solutions were dialyzed against 10 mM Tris/HCl buffer overnight using dialysis membranes with a MW cutoff of 6–8 kDa (Spectra/Por, Thermo Fisher Scientific GmbH, Germany). While eADF4(C16) and eADF4(κ16) variants were dialyzed at RT,[21b] dialysis of eADF4(Ω16) silk variants was conducted at 4 °C[21c] to reduce protein aggregation. For SDS-PAGE, proteins were incubated with Laemmli buffer (95 °C, 15 min) and analyzed using 5 µg protein, 12.5 % gels, and silver staining (n = 2). Since recombinant spider silk proteins contain Tyr but no Trp residues, potential *E. coli* contaminants could be identified by Trp fluorescence at 347 nm, because *E. coli* proteins comprised on average 1.5 % Trp residues.[21a,31] Fluorescence spectra were recorded using a FP 6500 spectrofluorimeter (Jasco, Japan) and protein concentrations of 0.5 mg mL^{-1}, black cuvettes, a step size of 0.5 nm and a scan speed of 100 nm min^{-1}. The excitation wavelength was either 275 nm (Tyr) or 295 nm (Trp), while the emission was recorded between 300 and 400 nm with bandwidths of 5 nm. Three spectra were recorded and averaged. As soluble spider silk proteins were unstructured, far-UV CD spectroscopy between 190 and 300 nm was conducted to determine secondary structure.[21a] CD spectra were recorded in triplicates on a J-815 CD spectrometer (Jasco, Japan) using concentrations of 0.2 mg mL^{-1}, cuvettes with a path length of 0.1 cm, an integration time of 1 s, and a scan speed of 50 nm min^{-1}. Three spectra were recorded and averaged.

Spider Silk Film Preparation: For film casting, spider silk variants were dissolved in 1,1,1,3,3,3-hexafluoro-2-ispropanol (HFIP) at a concentration of 10 mg mL^{-1} at RT overnight. The needed volume of silk solution was adjusted to the corresponding area of the used nontreated polystyrene surface (Sarstedt or Nunc, Thermo Fisher Scientific, Germany) to obtain films containing 0.5 mg spider silk protein per cm^2 after solvent evaporation. Since cast spider silk films exhibit a mainly α-helical or random coil structure making them water soluble, post-treatment using ethanol vapor in a desiccator was conducted to induce a structural transition into water insoluble β-sheets.[54]

Gradient Film Production: Gradient films mimicking a biochemical signaling gradient were produced in a modified and adopted manner as described previously.[21f] Therefore, eADF4(C16) (cytophobic) and eADF4(C16)-RGD (cytophilic) were dissolved in HFIP (10 mg mL^{-1}). Two 1 mL gastight glass syringes with Luer-lock connection (Hamilton, series 1000, Germany) were connected to in-house built tubing systems (Braun GmbH, Germany and Scientific Commodities Inc., USA) and mixing units consisting of tube adapters (Braun GmbH, Germany) and conical polyethylene tips (Sarstedt, Germany) to enable protein blending according to the applied inverse flow profiles of a Nemesys S syringe pump system (Cetoni GmbH, Germany). Besides linear gradients with steps lasting from 0.1 s, blocks with 100% of the corresponding spider silk variant flanked the gradient ends. Gradient and control films were produced at a total flow rate of 400 µL h^{-1} on glass substrates (Thermo Fisher Scientific, Germany) fixed on a mobile unit of a Harvard syringe pump system (Model 33, Harvard Apparatus, USA) moving with a continuous speed of 0.16 mm s^{-1}. Generated films were post-treated using ethanol vapor.

Water Contact Angle Measurements: To analyze the surface wettability of spider silk films and polystyrene, static WCA measurements were conducted using a Surftens-universal tensiometer (OEG GmbH, Germany) and the sessile drop method at RT. After an equilibration time of 10 s, an image was recorded and the contact angle was analyzed. Five measurements per condition were conducted (n = 5) and averaged (e.g., mean ± standard deviation [SD]). Each individual droplet was also measured five times in the software and averaged.

Cell Culture: The following chemicals were used for different cell culture studies: DMEM (BioSell, Germany), RPMI 1640 (Roswell Park Memorial Institute, Sigma-Aldrich, Germany), Eagle's minimum essential medium (EMEM, ATCC, Germany), FCS (BioSell, Germany), GlutaMax (Gibco, Thermo Fisher Scientific, Germany), Gentamycin-Sulfate (Sigma-Aldrich, Germany), trypsin (BioSell, Germany), 1× PBS (Sigma-Aldrich, Germany), non-essential amino acids (NEAA, Sigma-Aldrich, Germany), and trypan blue (Sigma-Aldrich, Germany). Human skin BJ fibroblasts (CRL-2522, ATCC, USA) were cultured in EMEM supplemented with 10% v/v FCS, 1% v/v GlutaMax, and 0.1% v/v gentamycin sulfate. Human bone MG-63 osteosarcoma fibroblasts (CRL-1427, ATCC, USA) were cultured in EMEM supplemented with 10% v/v FCS, 1% v/v GlutaMax, 1 % v/v NEAA, and 0.1% v/v gentamycin sulfate. Mouse M-MSV Balb/3T3 fibroblasts (ECACC, Sigma-Aldrich, Germany), rat nerve B50 neuronal cells (ECACC, Sigma-Aldrich, Germany), mouse C2C12 myoblasts (CLR-1772, ATCC, USA), mouse-rat NG108-15 somatic cell hybrids from glio- and neuroblastoma (HB-12317, ATCC, USA), human skin HaCaT keratinocytes (DKFZ, CLS, Germany), and immature, bipolar rat RN 22 Schwann cells (ECACC, Sigma-Aldrich, Germany) were cultured in DMEM supplemented with 10% v/v FCS, 1% v/v GlutaMax, and 0.1% v/v gentamycin sulfate. Human HeLa epithelial cells from a cervix carcinoma (ACC 57, DSMZ, Germany) were cultured in RPMI 1640 supplemented with 10% v/v FCS, 1% v/v GlutaMax, and 0.1% v/v gentamycin sulfate. HUVEC from the human umbilical cord (INS-Cl-1002, InSCREENeX GmbH, Germany) were cultured in huVEC basal medium (INS-ME-1011) supplemented with 5.7 % v/v supplements (INS-ME-1011BS, both InSCREENeX GmbH, Germany) and 0.1 % v/v gentamycin sulfate in gelatine-coated cell culture flasks. hiPSC derived cardiomyocytes were provided by Tilman Esser and Prof. Felix B. Engel (Nephropathology, University Hospital Erlangen, Germany) and cultured as published previously.[21e]

All cell types were cultivated using a cell culture incubator (HeraCell, Thermo Fisher Scientific, Germany) at humidified conditions containing 5 % CO_2 at 37 °C. Sub-culturing of cells was conducted using trypsin, except for hiPSC-cardiomyocytes. The hiPSC-cardiomyocytes were differentiated from hiPSC as described previously and sub-cultured using accutase.[21e] Cell numbers and viability was determined using trypan blue and an automated cell counter (TC20, Bio-Rad Laboratories, Germany). Prior to use in cell culture, (gradient) films were UV-sterilized for 30 min and washed using 1× PBS.

Cell Adhesion Analysis on Gradient Films: Balb 3T3 fibroblasts were seeded at a density of 10 000 cells per cm^2 in FCS-containing DMEM and incubated for 2 or 4 h in a cell incubator at 37 °C to analyze the influence of increasing RGD-density on cell attachment. Three spider silk gradient films were analyzed per condition (n = 3), while glass, eADF4(C16), and eADF4(C16)-RGD surfaces served as controls. Light microscopical images were recorded using a Leica DM IL LED microscope and the appropriate LAS 4.8 software (Leica, Germany) before washing to visualize also non-attached cells. After washing, cells were fixed using 3.7 % v/v paraformaldehyde (PFA) in 1× PBS (30 min, ambient conditions) and permeabilized using 0.1% v/v Triton X-100 in 1× PBS

(20 min, ambient conditions). Afterwards, the cell nuclei and the F-actin cytoskeleton were fluorescently stained (60 min, dark, RT) using 300 nM 4′,6-diamidino-2-phenylindole dihydrochloride (DAPI, Sigma-Aldrich, Germany) and 200 nM phalloidin tetramethyl rhodamine B isothiocyanate (Phalloidin-red, Sigma-Aldrich, Germany) in 1× PBS, respectively. Prior to imaging, the staining solution was exchanged with fresh 1× PBS. The gradient films were imaged using the DMI 8 confocal laser scanning microscope equipped with lasers using excitation wavelength of 405 nm (DAPI) and 552 nm (Phalloidin-red) and the appropriate LAS X software (Leica, Germany). Three individual gradient films were analyzed per incubation time ($n = 3$).

Cell Adhesion Assay for 4 h and Evaluation of Cell Adhesion Behavior: For each spider silk variant, three individual wells were analyzed with cells ($n = 3$), while untreated wells served as controls. To investigate the effect of added serum proteins, the cell adhesion behavior was analyzed in presence and absence of FCS. For each cell type, 10 000 cells per well (96 well plate) were seeded in 150 µL of the respective media and allowed to attach for 4 h at 37 °C. After 4 h, the cells were fixed, permeabilized, and fluorescently stained (300 nM DAPI and 200 nM Phalloidin-red) as mentioned above. To evaluate cell adhesion behavior, cell numbers as well as the morphology and spreading behavior of attached cells were analyzed using a Leica DMI 3000B fluorescence microscope with a 20× objective and the LAS X software (Leica, Germany). A high cell number combined with clear cell spreading and a visible, organized F-actin expression indicated a very good cell attachment (++) and classified the spider silk as cell-adhesive. As soon as the number of attached cells was reduced, but cell spreading was visible, or many cells were visible starting to form a F-actin cytoskeleton, the variant was classified as "good" (+). If a surface showed moderate number of attached cells, which formed some focal adhesions or stress fibers, indicated by some F-actin filaments, the respective spider silk variant showed moderate cell adhesion behavior (0). In contrast, spider silk variants showing few attached cells exhibiting a mainly round morphology without a clear F-actin cytoskeleton formation were classified as poor adhesive surfaces (−). As soon as only a few sporadic round cells were detectable showing no or less F-actin expression, the cell attachment was very poor (−), and the silk surfaces were classified as a cell-repellent. Furthermore, cell numbers of four selected, representative fluorescence images ($n = 4$) per condition (eADF4(C16), eADF4(C16)-RGD, eADF4(C16)-KGD) were counted for every cell line and summed up to quantify cell adhesion behavior on these spider silk variants.

Co-Culture for Selective Attachment: To demonstrate spider silk selective cell attachment, co-culture experiments using mouse C2C12 myoblasts and rat B50 neuronal cells were conducted on eADF4(C16)-KGD (cell-specific for C2C12 myoblasts) and eADF4(C16)-RGD (cytophilic) spider silk films. C2C12 myoblasts and B50 neuronal cells were stained with Syto 9 DNA stain (green, Invitrogen, Thermo Fisher Scientific, Germany) and CellTracker Red CMTPX (red, Invitrogen, Thermo Fisher Scientific, Germany), respectively, to enable specific recognition of the respective cell type using fluorescence microscopy afterwards ($n = 3$). Confluent cells were incubated with 1 µM DNA stain or cell mask in DMEM for 1 h. Afterwards, both cell layers were washed several times using 1× PBS to remove excess surface bound dye. After sub-culturing using trypsin, cells were resuspended in DMEM without FCS, and 10 000 cells per cm^2 were seeded on eADF4(C16)-KGD and eADF4(C16)-RGD films. Wells without spider silk films and individually cultured cells on silk films served as control. The staining success was verified using a Leica DMI 3000B fluorescence microscope equipped with a 10× and a 20× objective and the LAS X software (Leica, Germany). Fluorescence microscopy was conducted at different timepoints ($t = 0$, 2, 4, and 6 h) before and after washing (1× PBS) to check cell adhesion behavior. After washing, FCS-containing DMEM FCS was added. To confirm cell selectivity of eADF4(C16)-KGD compared to eADF4(C16)-RGD, the same samples were imaged again using fluorescence microscopy on the next day.

Cell Proliferation Assay: A proliferation assay over 8 days was conducted on spider silk films made of eADF4(C16) (cytophobic), eADF4(C16)-RGD (cytophilic), and eADF4(C16)-KGD (cell-specific for C2C12 myoblasts) using seven different cell types (mouse C2C12 myoblasts, human BJ fibroblasts, human HaCaT keratinocytes, human MG63 osteosarcoma fibroblasts, rat RN22 Schwann cells, rat B50 neuronal cells, and mouse-rat NG108-15 somatic hybrid cells). For each spider silk variant, four different wells were analyzed ($n = 4$) and averaged (e.g., mean ± SD), while wells without films served as controls. For each cell type, 5000 cells per 1 cm^2 were seeded in 150 µL media containing 10% FCS and incubated at 37 °C. To evaluate cell proliferation, a CellTiter-Blue cell viability assay (Promega, USA) was conducted on day 1, 3 or 4, 6, and 8. After washing using 1× PBS, 150 µL of 10% v/v CellTiter-Blue reagent in the respective cell culture media were added and incubated for 2.5 h. Samples without cells served as blanks to determine self-degradation of resazurin over time. The averaged blank samples were subtracted from the measured values. The viability of cells could be determined by their metabolic turnover of resazurin (blue) to resofurin (pink, $\lambda_{ex} = 530$ nm, $\lambda_{em} = 590$ nm) by viable cells. Therefore, 100 µL of respective supernatants were transferred to a black 96 well plate (Nunc, Thermo Fisher Scientific, Germany) and measured at 590 nm using a plate reader system (Mithras LB940, Berthold Technologies, Germany).

Statistical Analysis: A pre-processing of the data was not performed. The respective information about sample sizes and data presentation was added at the appropriate experimental procedures. Further statistical analyses were not conducted.

Supporting Information

Supporting Information is available from the Wiley Online Library or from the author.

Acknowledgements

The authors acknowledge the funding from the Deutsche Forschungsgemeinschaft (DFG, German Research Foundation)—project number 326998133-TRR225 (funded sub-project: C01). Support from the Elite Network of Bavaria is also acknowledged. The authors thank Andreas Schmidt, Johannes Diehl, Andreas Kumschier, Comfort Ajala, Vivien Beyersdorfer, Kathrin Döhla, and Thomas Göbbel for supporting protein production and purification. Andreas Schmidt is also acknowledged for MALDI-TOF measurements. Alexandra Pellert, Eva Möller, and Nicole Pittel are acknowledged for supporting cell culture. The authors also want to thank Christina Heinritz for assistance in gradient film generation and Dr. Vanessa Neubauer for critical discussions. Final thanks to Prof. Felix B. Engel and Tilman Esser for providing hiPSC-derived cardiomyocytes.

Open access funding enabled and organized by Projekt DEAL.

Conflict of Interest

T.S. is co-founder and shareholder of AMSilk GmbH.

Data Availability Statement

The data that support the findings of this study are available from the corresponding author upon reasonable request.

Keywords

bioactive peptides, bioselectivity, cell co-culture, cytophilic surfaces, gradient materials

Received: October 14, 2022
Revised: December 19, 2022
Published online: January 13, 2023

[1] a) G. Huang, F. Li, X. Zhao, Y. Ma, Y. Li, M. Lin, G. Jin, T. J. Lu, G. M. Genin, F. Xu, *Chem. Rev.* **2017**, *117*, 12764; b) D. T. Scadden, *Nature* **2006**, *441*, 1075.

[2] a) J. Engel, M. Chiquet, in *The Extracellular Matrix: An Overview* (Ed: R. P. Mecham), Springer, Berlin **2011**, p. 1; b) A. D. Theocharis, S. S. Skandalis, C. Gialeli, N. K. Karamanos, *Adv. Drug Delivery Rev.* **2016**, *97*, 4; c) W. P. Daley, S. B. Peters, M. Larsen, *J. Cell Sci.* **2008**, *121*, 255.

[3] D. E. Discher, D. J. Mooney, P. W. Zandstra, *Science* **2009**, *324*, 1673.

[4] a) R. Langer, J. P. Vacanti, *Science* **1993**, *260*, 920; b) J. L. Carvalho, P. H. de Carvalho, D. A. Gomes, A. M. de Goes, *Adv. Biomater. Sci. Biomed. Appl.* **2013**, *11*, 295; c) C. A. Vacanti, J. P. Vacanti, *Surg. Technol. Int.* **1991**, *I*, 43; d) U. A. Stock, J. P. Vacanti, *Annu. Rev. Med.* **2001**, *52*, 443.

[5] a) B. P. Chan, K. W. Leong, *Eur. Spine J.* **2008**, *17*, 467; b) S. Hinderer, S. L. Layland, K. Schenke-Layland, *Adv. Drug Delivery Rev.* **2016**, *97*, 260; c) F. J. O'Brien, *Mater. Today* **2011**, *14*, 88; d) S. M. Choi, P. Chaudhry, S. M. Zo, S. S. Han, in *Cutting-Edge Enabling Technologies for Regenerative Medicine* (Eds: H. J. Chun, C. H. Park, I. K. Kwon, G. Khang), Springer, Singapore **2018**, p. 161; e) S. Pacelli, V. Manoharan, A. Desalvo, N. Lomis, K. S. Jodha, S. Prakash, A. Paul, *J. Mater. Chem. B* **2016**, *4*, 1586; f) M. Pagel, A. G. Beck-Sickinger, *Biol. Chem.* **2017**, *398*, 3; g) K. Borcherding, G. Schmidmaier, G. O. Hofmann, B. Wildemann, *Injury* **2021**, *52*, S106; h) X. Zhao, in *Bioactive Materials in Medicine* (Eds: X. Zhao, J. M. Courtney, H. Qian), Woodhead Publishing, Cambridge, UK **2011**, p. 1; i) J. Najdanović, J. Rajković, S. Najman, in *Biomaterials in Clinical Practice: Advances in Clinical Research and Medical Devices* (Eds: F. Zivic, S. Affatato, M. Trajanovic, M. Schnabelrauch, N. Grujovic, K. L. Choy), Springer International Publishing, Cham **2018**, p. 333; j) S. Spiller, F. Clauder, K. Bellmann-Sickert, A. G. Beck-Sickinger, *Biol. Chem.* **2021**, *402*, 1271.

[6] a) J. A. DeQuach, V. Mezzano, A. Miglani, S. Lange, G. M. Keller, F. Sheikh, K. L. Christman, *PLoS One* **2010**, *5*, e13039; b) Y. Zhang, Y. He, S. Bharadwaj, N. Hammam, K. Carnagey, R. Myers, A. Atala, M. Van Dyke, *Biomaterials* **2009**, *30*, 4021; c) D. Lam, H. A. Enright, J. Cadena, S. K. G. Peters, A. P. Sales, J. J. Osburn, D. A. Soscia, K. S. Kulp, E. K. Wheeler, N. O. Fischer, *Sci. Rep.* **2019**, *9*, 4159; d) D. Olvera, B. N. Sathy, D. J. Kelly, *ACS Biomater. Sci. Eng.* **2020**, *6*, 5145; e) A. Shridhar, B. G. Amsden, E. R. Gillies, L. E. Flynn, *Front. Bioeng. Biotechnol.* **2019**, *7*, 402.

[7] a) A.-S. Mertgen, V. T. Trossmann, A. G. Guex, K. Maniura-Weber, T. Scheibel, M. Rottmar, *ACS Appl. Mater. Interfaces* **2020**, *12*, 21342; b) K. Kyzioł, Ł. Kaczmarek, A. Kyzioł, in *Handbook of Composites from Renewable Materials* (Eds: V. K. Thakur, M. K. Thakur, M. R. Kessler), Scrivener Publishing, Beverly, MA **2017**, p. 457; c) R. Fraioli, S. Neubauer, F. Rechenmacher, B. M. Bosch, K. Dashnyam, J. H. Kim, R. A. Perez, H. W. Kim, F. J. Gil, M. P. Ginebra, J. M. Manero, H. Kessler, C. Mas-Moruno, *Biomater. Sci.* **2019**, *7*, 1281; d) H. Zhang, X. Zheng, W. Ahmed, Y. Yao, J. Bai, Y. Chen, C. Gao, *Biomacromolecules* **2018**, *19*, 1746.

[8] a) P. Jurczak, J. Witkowska, S. Rodziewicz-Motowidło, S. Lach, *Adv. Colloid Interface Sci.* **2020**, *276*, 102083; b) H. Amani, H. Arzaghi, M. Bayandori, A. S. Dezfuli, H. Pazoki-Toroudi, A. Shafiee, L. Moradi, *Adv. Mater. Interfaces* **2019**, *6*, 1900572; c) A. Cipitria, M. Salmeron-Sanchez, *Adv. Healthcare Mater.* **2017**, *6*, 1700052; d) J. A. Hubbell, *Curr. Opin. Biotechnol.* **1999**, *10*, 123; e) N. R. Richbourg, N. A. Peppas, V. I. Sikavitsas, *J. Tissue Eng. Regener. Med.* **2019**, *13*, 1275; f) M. Salmerón-Sánchez, M. J. Dalby, *Chem. Commun.* **2016**, *52*, 13327; g) K. Hosoyama, C. Lazurko, M. Muñoz, C. D. McTiernan, E. I. Alarcon, *Front. Bioeng. Biotechnol.* **2019**, *7*, 205; h) N. Huettner, T. R. Dargaville, A. Forget, *Trends Biotechnol.* **2018**, *36*, 372.

[9] a) E. Ruoslahti, M. D. Pierschbacher, *Cell* **1986**, *44*, 517; b) M. D. Pierschbacher, E. Ruoslahti, *Nature* **1984**, *309*, 30; c) M. D. Pierschbacher, E. G. Hayman, E. Ruoslahti, *J. Cell. Biochem.* **1985**, *28*, 115; d) M. D. Pierschbacher, E. Ruoslahti, *Proc. Natl. Acad. Sci. USA* **1984**, *81*, 5985.

[10] a) S. L. Bellis, *Biomaterials* **2011**, *32*, 4205; b) U. Hersel, C. Dahmen, H. Kessler, *Biomaterials* **2003**, *24*, 4385.

[11] a) M. Pfaff, in *Integrin-Ligand Interaction*, Springer, Boston, MA **1997**, p. 101; b) T. G. Kapp, F. Rechenmacher, S. Neubauer, O. V. Maltsev, E. A. Cavalcanti-Adam, R. Zarka, U. Reuning, J. Notni, H.-J. Wester, C. Mas-Moruno, J. Spatz, B. Geiger, H. Kessler, *Sci. Rep.* **2017**, *7*, 39805; c) W. M. Han, Y. C. Jang, A. J. García, in *Biomaterials Science*, 4th ed. (Eds: W. R. Wagner, S. E. Sakiyama-Elbert, G. Zhang, M. J. Yaszemski), Academic Press, Cambridge, MA, USA **2020**, p. 701.

[12] a) E. Ruoslahti, *Annu. Rev. Cell Dev. Biol.* **1996**, *12*, 697; b) K. G. Sreejalekshmi, P. D. Nair, *J. Biomed. Mater. Res., Part A* **2011**, *96A*, 477; c) F. R. Maia, S. J. Bidarra, P. L. Granja, C. C. Barrias, *Acta Biomater.* **2013**, *9*, 8773; d) J. Xu, D. Mosher, in *The Extracellular Matrix: An Overview* (Ed: R. P. Mecham), Springer, Berlin **2011**, p. 41; e) B. K. Mann, A. T. Tsai, T. Scott-Burden, J. L. West, *Biomaterials* **1999**, *20*, 2281; f) K. M. Yamada, *J. Biol. Chem.* **1991**, *266*, 12809.

[13] a) K. Tashiro, G. C. Sephel, B. Weeks, M. Sasaki, G. R. Martin, H. K. Kleinman, Y. Yamada, *J. Biol. Chem.* **1989**, *264*, 16174; b) Y. Yin, W. Wang, Q. Shao, B. Li, D. Yu, X. Zhou, J. Parajuli, H. Xu, T. Qiu, A. K. Yetisen, N. Jiang, *Biomater. Sci.* **2021**, *9*, 2887; c) R. Patel, M. Santhosh, J. K. Dash, R. Karpoormath, A. Jha, J. Kwak, M. Patel, J. H. Kim, *Polym. Adv. Technol.* **2019**, *30*, 4; d) T. H. Perera, S. M. Howell, L. A. S. Callahan, *Biomacromolecules* **2019**, *20*, 3009; e) W. Sun, T. Incitti, C. Migliaresi, A. Quattrone, S. Casarosa, A. Motta, *J. Tissue Eng. Regener. Med.* **2017**, *11*, 1532.

[14] a) S. P. Massia, S. S. Rao, J. A. Hubbell, *J. Biol. Chem.* **1993**, *268*, 8053; b) J. Graf, Y. Iwamoto, M. Sasaki, G. R. Martin, H. K. Kleinman, F. A. Robey, Y. Yamada, *Cell* **1987**, *48*, 989; c) J. Graf, R. C. Ogle, F. A. Robey, M. Sasaki, G. R. Martin, Y. Yamada, H. K. Kleinman, *Biochemistry* **1987**, *26*, 6896; d) H.-W. Jun, J. West, *J. Biomater. Sci., Polym. Ed.* **2004**, *15*, 73.

[15] a) R. M. Scarborough, J. W. Rose, M. A. Hsu, D. R. Phillips, V. A. Fried, A. M. Campbell, L. Nannizzi, I. F. Charo, *J. Biol. Chem.* **1991**, *266*, 9359; b) P. Nykvist, K. Tasanen, T. Viitasalo, J. Käpylä, J. Jokinen, L. Bruckner-Tuderman, J. Heino, *J. Biol. Chem.* **2001**, *276*, 38673; c) H. Minoux, C. Chipot, D. Brown, B. Maigret, *J. Comput.-Aided Mol. Des.* **2000**, *14*, 317; d) J. Salber, S. Gräter, M. Harwardt, M. Hofmann, D. Klee, J. Dujic, H. Jinghuan, J. Ding, S. Kippenberger, A. Bernd, J. Groll, J. P. Spatz, M. Möller, *Small* **2007**, *3*, 1023.

[16] a) C. G. Knight, L. F. Morton, A. R. Peachey, D. S. Tuckwell, R. W. Farndale, M. J. Barnes, *J. Biol. Chem.* **2000**, *275*, 35; b) W.-M. Zhang, J. Käpylä, J. S. Puranen, C. G. Knight, C.-F. Tiger, O. T. Pentikäinen, M. S. Johnson, R. W. Farndale, J. Heino, D. Gullberg, *J. Biol. Chem.* **2003**, *278*, 7270.

[17] a) N. T. Feric, C. C. H. Cheng, M. C. Goh, V. Dudnyk, V. Di Tizio, M. Radisic, *Biomater. Sci.* **2014**, *2*, 1384; b) L. A. Reis, L. L. Y. Chiu, J. Wu, N. Feric, C. Laschinger, A. Momen, R.-K. Li, M. Radisic, *Circ.: Heart Failure* **2015**, *8*, 333; c) J. W. Miklas, S. M. Dallabrida, L. A. Reis, N. Ismail, M. Rupnick, M. Radisic, *PLoS One* **2013**, *8*, e72956.

[18] a) J. A. Hubbell, S. P. Massia, N. P. Desai, P. D. Drumheller, *Bio/Technology* **1991**, *9*, 568; b) S. P. Massia, J. A. Hubbell, *J. Biol. Chem.* **1992**, *267*, 14019; c) Y. Liu, A. Mahara, Y. Kambe, Y.-I. Hsu, T. Yamaoka, *Biomater. Sci.* **2021**, *9*, 1034.

[19] a) M. Mehta, C. M. Madl, S. Lee, G. N. Duda, D. J. Mooney, *J. Biomed. Mater. Res., Part A* **2015**, *103*, 3516; b) A. Jha, E. Moore, *J. Mater. Res.* **2021**, *37*, 77.

[20] a) T. B. Aigner, E. DeSimone, T. Scheibel, *Adv. Mater.* **2018**, *30*, 1704636; b) S. Salehi, K. Koeck, T. Scheibel, *Molecules* **2020**, *25*, 737; c) A. Leal-Egaña, T. Scheibel, *Biotechnol. Appl. Biochem.* **2010**, *55*, 155.

[21] a) D. Huemmerich, C. W. Helsen, S. Quedzuweit, J. Oschmann, R. Rudolph, T. Scheibel, *Biochemistry* **2004**, *43*, 13604; b) E. Doblhofer, T. Scheibel, *J. Pharm. Sci.* **2015**, *104*, 988; c) S. Kumari, G. Lang, E.

DeSimone, C. Spengler, V. T. Trossmann, S. Lücker, M. Hudel, K. Jacobs, N. Krämer, T. Scheibel, *Mater. Today* **2020**, *41*, 21; d) S. Kumari, G. Lang, E. DeSimone, C. Spengler, V. T. Trossmann, S. Lücker, M. Hudel, K. Jacobs, N. Krämer, T. Scheibel, *Data Brief* **2020**, *32*, 106305; e) T. U. Esser, V. T. Trossmann, S. Lentz, F. B. Engel, T. Scheibel, *Mater Today Bio* **2021**, *11*, 100114; f) V. J. Neubauer, T. Scheibel, *ACS Biomater. Sci. Eng.* **2020**, *6*, 5599; g) S. Wohlrab, S. Müller, A. Schmidt, S. Neubauer, H. Kessler, A. Leal-Egaña, T. Scheibel, *Biomaterials* **2012**, *33*, 6650; h) M. B. Elsner, H. M. Herold, S. Müller-Herrmann, H. Bargel, T. Scheibel, *Biomater. Sci.* **2015**, *3*, 543.

[22] J. D. Humphries, A. Byron, M. J. Humphries, *J. Cell Sci.* **2006**, *119*, 3901.

[23] a) T.-Y. Cheng, M.-H. Chen, W.-H. Chang, M.-Y. Huang, T.-W. Wang, *Biomaterials* **2013**, *34*, 2005; b) T. H. Perera, X. Lu, L. A. S. Callahan, *J. Funct. Biomater.* **2020**, *11*, 15; c) A. Farrukh, S. Zhao, A. del Campo, *Front. Mater.* **2018**, *5*, 62; d) A. Farrukh, J. I. Paez, M. Salierno, W. Fan, B. Berninger, A. del Campo, *Biomacromolecules* **2017**, *18*, 906; e) A. Farrukh, F. Ortega, W. Fan, N. Marichal, J. I. Paez, B. Berninger, A. d. Campo, M. J. Salierno, *Stem Cell Rep.* **2017**, *9*, 1432; f) S. K. Powell, J. Rao, E. Roque, M. Nomizu, Y. Kuratomi, Y. Yamada, H. K. Kleinman, *J. Neurosci. Res.* **2000**, *61*, 302; g) M. Nomizu, B. S. Weeks, C. A. Weston, W. H. Kim, H. K. Kleinman, Y. Yamada, *FEBS Lett.* **1995**, *365*, 227; h) M. Yamada, Y. Kadoya, S. Kasai, K. Kato, M. Mochizuki, N. Nishi, N. Watanabe, H. K. Kleinman, Y. Yamada, M. Nomizu, *FEBS Lett.* **2002**, *530*, 48; i) R. A. Que, J. Arulmoli, N. A. Da Silva, L. A. Flanagan, S.-W. Wang, *J. Biomed. Mater. Res., Part A* **2018**, *106*, 1363; j) Y. Wu, Q. Zheng, J. Du, Y. Song, B. Wu, X. Guo, *J. Huazhong Univ. Sci. Technol., Med. Sci.* **2006**, *26*, 594; k) I. C. Yasa, N. Gunduz, M. Kilinc, M. O. Guler, A. B. Tekinay, *Sci. Rep.* **2015**, *5*, 16460; l) M. Widhe, U. Johansson, C.-O. Hillerdahl, M. Hedhammar, *Biomaterials* **2013**, *34*, 8223; m) G. A. Silva, C. Czeisler, K. L. Niece, E. Beniash, D. A. Harrington, J. A. Kessler, S. I. Stupp, *Science* **2004**, *303*, 1352; n) B. Li, T. Qiu, P. Zhang, X. Wang, Y. Yin, S. Li, *Cell Proliferation* **2014**, *47*, 133; o) E. Sieni, B. Bazzolo, F. Pieretti, A. Zamuner, A. Tasso, M. Dettin, M. T. Conconi, *Bioelectrochemistry* **2020**, *136*, 107626.

[24] a) M. Matsuzawa, F. F. Weight, R. S. Potember, P. Liesi, *Int. J. Dev. Neurosci.* **1996**, *14*, 283; b) M. J. Cooke, T. Zahir, S. R. Phillips, D. S. Shah, D. Athey, J. H. Lakey, M. S. Shoichet, S. A. Przyborski, *J. Biomed. Mater. Res., Part A* **2010**, *93*, 824; c) W. Wang, L. Guo, Y. Yu, Z. Chen, R. Zhou, Z. Yuan, *J. Biomed. Mater. Res., Part A* **2015**, *103*, 1703; d) Y. Iwamoto, F. A. Robey, J. Graf, M. Sasaki, H. K. Kleinman, Y. Yamada, G. R. Martin, *Science* **1987**, *238*, 1132; e) G. Sarfati, T. Dvir, M. Elkabets, R. N. Apte, S. Cohen, *Biomaterials* **2011**, *32*, 152.

[25] a) F. Rask, S. M. Dallabrida, N. S. Ismail, Z. Amoozgar, Y. Yeo, M. A. Rupnick, M. Radisic, *J. Biomed. Mater. Res., Part A* **2010**, *95A*, 105; b) F. Rask, A. Mihic, L. Reis, S. M. Dallabrida, N. S. Ismail, K. Sider, C. A. Simmons, M. A. Rupnick, R. D. Weisel, R.-K. Li, M. Radisic, *Soft Matter* **2010**, *6*, 5089; c) L. A. Reis, L. L. Y. Chiu, Y. Liang, K. Hyunh, A. Momen, M. Radisic, *Acta Biomater.* **2012**, *8*, 1022; d) H. Cai, F.-Y. Wu, Q.-L. Wang, P. Xu, F.-F. Mou, S.-J. Shao, Z.-R. Luo, J. Zhu, S.-S. Xuan, R. Lu, H.-D. Guo, *FASEB J.* **2019**, *33*, 8306; e) S. Mandla, L. D. Huyer, Y. Wang, M. Radisic, *ACS Biomater. Sci. Eng.* **2019**, *5*, 4542; f) Y. Xiao, L. A. Reis, N. Feric, E. J. Knee, J. Gu, S. Cao, C. Laschinger, C. Londono, J. Antolovich, A. P. McGuigan, M. Radisic, *Proc. Natl. Acad. Sci. USA* **2016**, *113*, E5792; g) L. T. Dang, N. T. Feric, C. Laschinger, W. Y. Chang, B. Zhang, G. A. Wood, W. L. Stanford, M. Radisic, *Biomaterials* **2014**, *35*, 7786.

[26] a) K. Oshikawa, S. Terada, *J. Biochem.* **1999**, *125*, 31; b) K. Tasanen, J. A. Eble, M. Aumailley, H. Schumann, J. Baetge, H. Tu, P. Bruckner, L. Bruckner-Tuderman, *J. Biol. Chem.* **2000**, *275*, 3093.

[27] a) R. Mhanna, E. Öztürk, Q. Vallmajo-Martin, C. Millan, M. Müller, M. Zenobi-Wong, *Tissue Eng., Part A* **2014**, *20*, 1165; b) P. Castillo-Briceño, D. Bihan, M. Nilges, S. Hamaia, J. Meseguer, A. García-Ayala, R. W. Farndale, V. Mulero, *Mol. Immunol.* **2011**, *48*, 826.

[28] a) H.-B. Lin, W. Sun, D. F. Mosher, C. García-Echeverría, K. Schaufelberger, P. I. Lelkes, S. L. Cooper, *J. Biomed. Mater. Res.* **1994**, *28*, 329; b) H.-B. Lin, C. García-Echeverría, S. Asakura, W. Sun, D. F. Mosher, S. L. Cooper, *Biomaterials* **1992**, *13*, 905.

[29] a) G. L. Rosano, E. A. Ceccarelli, *Front. Microbiol.* **2014**, *5*, 172; b) S. Sahdev, S. K. Khattar, K. S. Saini, *Mol. Cell. Biochem.* **2008**, *307*, 249.

[30] S. Hosseini, S. O. Martinez-Chapa, in *Fundamentals of MALDI-ToF-MS Analysis: Applications in Bio-diagnosis Tissue Engineering and Drug Delivery*, Springer, Singapore **2017**, p. 1.

[31] F. R. Blattner, G. Plunkett 3rd, C. A. Bloch, N. T. Perna, V. Burland, M. Riley, J. Collado-Vides, J. D. Glasner, C. K. Rode, G. F. Mayhew, J. Gregor, N. W. Davis, H. A. Kirkpatrick, M. A. Goeden, D. J. Rose, B. Mau, Y. Shao, *Science* **1997**, *277*, 1453.

[32] K. Spieß, S. Wohlrab, T. Scheibel, *Soft Matter* **2010**, *6*, 4168.

[33] J. Petzold, T. B. Aigner, F. Touska, K. Zimmermann, T. Scheibel, F. B. Engel, *Adv. Funct. Mater.* **2017**, *27*, 1701427.

[34] S. Wohlrab, K. Spieß, T. Scheibel, *J. Mater. Chem.* **2012**, *22*, 22050.

[35] a) J. G. Steele, G. Johnson, W. D. Norris, P. A. Underwood, *Biomaterials* **1991**, *12*, 531; b) P. A. Underwood, F. A. Bennett, *J. Cell Sci.* **1989**, *93*, 641; c) P. A. Underwood, P. A. Bean, *Cells Mater.* **1996**, *6*, 20; d) P. A. Underwood, P. A. Bean, S. M. Mitchell, J. M. Whitelock, *J. Immunol. Methods* **2001**, *247*, 217; e) M. Widhe, N. D. Shalaly, M. Hedhammar, *Biomaterials* **2016**, *74*, 256; f) M. Widhe, H. Bysell, S. Nystedt, I. Schenning, M. Malmsten, J. Johansson, A. Rising, M. Hedhammar, *Biomaterials* **2010**, *31*, 9575.

[36] a) D. Steiner, S. Winkler, S. Heltmann-Meyer, V. T. Trossmann, T. Fey, T. Scheibel, R. E. Horch, A. Arkudas, *Biofabrication* **2021**, *13*, 045003; b) P. H. Zeplin, N. C. Maksimovikj, M. C. Jordan, J. Nickel, G. Lang, A. H. Leimer, L. Römer, T. Scheibel, *Adv. Funct. Mater.* **2014**, *24*, 2658; c) M. Lucke, I. Mottas, T. Herbst, C. Hotz, L. Römer, M. Schierling, H. M. Herold, U. Slotta, T. Spinetti, T. Scheibel, G. Winter, C. Bourquin, J. Engert, *Biomaterials* **2018**, *172*, 105.

[37] a) A. Leal-Egaña, G. Lang, C. Mauerer, J. Wickinghoff, M. Weber, S. Geimer, T. Scheibel, *Adv. Eng. Mater.* **2012**, *14*, B67; b) C. B. Borkner, S. Wohlrab, E. Möller, G. Lang, T. Scheibel, *ACS Biomater. Sci. Eng.* **2017**, *3*, 767; c) P. H. Zeplin, A.-K. Berninger, N. C. Maksimovikj, P. Van Gelder, T. Scheibel, H. Walles, *Handchirurgie Mikrochirurgie Plastische Chirurgie* **2014**, *46*, 336.

[38] I. Pountos, M. Panteli, A. Lampropoulos, E. Jones, G. M. Calori, P. V. Giannoudis, *BMC Med.* **2016**, *14*, 103.

[39] a) J. P. M. Kramer, T. B. Aigner, J. Petzold, K. Roshanbinfar, T. Scheibel, F. B. Engel, *Sci. Rep.* **2020**, *10*, 8789; b) K. Schacht, T. Jüngst, M. Schweinlin, A. Ewald, J. Groll, T. Scheibel, *Angew. Chem., Int. Ed.* **2015**, *54*, 2816.

[40] a) E. Bini, C. W. P. Foo, J. Huang, V. Karageorgiou, B. Kitchel, D. L. Kaplan, *Biomacromolecules* **2006**, *7*, 3139; b) J. Zhao, H. Qiu, D.-l. Chen, W.-x. Zhang, D.-c. Zhang, M. Li, *Int. J. Biol. Macromol.* **2013**, *56*, 106; c) M. Widhe, J. Johansson, M. Hedhammar, A. Rising, *Biopolymers* **2012**, *97*, 468; d) C. P. Tasiopoulos, L. Gustafsson, W. van der Wijngaart, M. Hedhammar, *ACS Biomater. Sci. Eng.* **2021**, *7*, 3332; e) C. P. Tasiopoulos, M. Widhe, M. Hedhammar, *ACS Appl. Mater. Interfaces* **2018**, *10*, 14531; f) C. P. Tasiopoulos, S. Petronis, H. Sahlin, M. Hedhammar, *ACS Appl. Bio Mater.* **2020**, *3*, 577.

[41] a) A. Lagunas, J. Comelles, E. Martínez, E. Prats-Alfonso, G. A. Acosta, F. Albericio, J. Samitier, *Nanomedicine* **2012**, *8*, 432; b) B. P. Harris, J. K. Kutty, E. W. Fritz, C. K. Webb, K. J. L. Burg, A. T. Metters, *Langmuir* **2006**, *22*, 4467; c) X. Tong, J. Jiang, D. Zhu, F. Yang, *ACS Biomater. Sci. Eng.* **2016**, *2*, 845.

[42] a) V. T. Trossmann, S. Heltmann-Meyer, H. Amouei, H. Wajant, R. E. Horch, D. Steiner, T. Scheibel, *Biomacromolecules* **2022**, *23*, 4427; b) A. Lechner, V. T. Trossmann, T. Scheibel, *Macromol. Biosci.* **2021**, *22*, 2100390.

[43] S. Lentz, V. T. Trossmann, C. B. Borkner, V. Beyersdorfer, M. Rottmar, T. Scheibel, *ACS Appl. Mater. Interfaces* **2022**, *14*, 31751.

[44] a) A. Leal-Egana, A. Díaz-Cuenca, A. Boccaccini, *Adv. Mater.* **2013**, *25*, 4049; b) A. Blau, *Curr. Opin. Colloid Interface Sci.* **2013**, *18*, 481; c) M. De Rosa, M. Carteni', O. Petillo, A. Calarco, S. Margarucci, F. Rosso, A. De Rosa, E. Farina, P. Grippo, G. Peluso, *J. Cell. Physiol.* **2004**, *198*, 133.
[45] U. Johansson, M. Ria, K. Åvall, N. D. Shalaly, S. V. Zaitsev, P.-O. Berggren, M. Hedhammar, *PLoS One* **2015**, *10*, e0130169.
[46] a) M. Barczyk, S. Carracedo, D. Gullberg, *Cell Tissue Res.* **2009**, *339*, 269; b) O. Schussler, J. C. Chachques, M. Alifano, Y. Lecarpentier, *J. Cardiovasc. Transl. Res.* **2021**, *15*, 179.
[47] J. Heino, *BioEssays* **2007**, *29*, 1001.
[48] R. A. Lazarus, R. S. McDowell, *Curr. Opin. Biotechnol.* **1993**, *4*, 438.
[49] M. D. Pierschbacher, E. Ruoslahti, *J. Biol. Chem.* **1987**, *262*, 17294.
[50] a) T. Sasagawa, T. Shimizu, S. Sekiya, Y. Haraguchi, M. Yamato, Y. Sawa, T. Okano, *Biomaterials* **2010**, *31*, 1646; b) D. W. van der Schaft, A. C. van Spreeuwel, H. C. van Assen, F. P. Baaijens, *Tissue Eng., Part A* **2011**, *17*, 2857.
[51] S. T. Cooper, A. L. Maxwell, E. Kizana, M. Ghoddusi, E. C. Hardeman, I. E. Alexander, D. G. Allen, K. N. North, *Cell Motil. Cytoskeleton* **2004**, *58*, 200.
[52] a) S. Ostrovidov, S. Ahadian, J. Ramon-Azcon, V. Hosseini, T. Fujie, S. P. Parthiban, H. Shiku, T. Matsue, H. Kaji, M. Ramalingam, H. Bae, A. Khademhosseini, *J. Tissue Eng. Regener. Med.* **2017**, *11*, 582; b) M. Das, J. W. Rumsey, N. Bhargava, M. Stancescu, J. J. Hickman, *Biomaterials* **2010**, *31*, 4880; c) J. X. Jiang, R. C. Choi, N. L. Siow, H. H. Lee, D. C. Wan, K. W. Tsim, *J. Biol. Chem.* **2003**, *278*, 45435; d) M. Das, J. W. Rumsey, C. A. Gregory, N. Bhargava, J. F. Kang, P. Molnar, L. Riedel, X. Guo, J. J. Hickman, *Neuroscience* **2007**, *146*, 481; e) M. Das, J. W. Rumsey, N. Bhargava, M. Stancescu, J. J. Hickman, *Biomaterials* **2009**, *30*, 5392; f) X. Guo, M. Gonzalez, M. Stancescu, H. H. Vandenburgh, J. J. Hickman, *Biomaterials* **2011**, *32*, 9602; g) A. S. Smith, S. L. Passey, N. R. Martin, D. J. Player, V. Mudera, L. Greensmith, M. P. Lewis, *Cells Tissues Organs* **2016**, *202*, 143; h) J. W. Santoso, X. Li, D. Gupta, G. C. Suh, E. Hendricks, S. Lin, S. Perry, J. K. Ichida, D. Dickman, M. L. McCain, *APL Bioeng.* **2021**, *5*, 036101.
[53] a) E. DeSimone, K. Schacht, A. Pellert, T. Scheibel, *Biofabrication* **2017**, *9*, 044104; b) K. Schacht, T. Scheibel, *Biomacromolecules* **2011**, *12*, 2488.
[54] K. Spiess, R. Ene, C. D. Keenan, J. Senker, F. Kremer, T. Scheibel, *J. Mater. Chem.* **2011**, *21*, 13594.